

Building Damage Detection using SAR Images in the 2010 Haiti Earthquake



15 WCEE
LSBOA 2012

Pralhad Uprety and Fumio Yamazaki

Department of Urban environment System, Chiba University, Japan

SUMMARY

Radar remote sensing, as in SAR, is an independent of daylight and cloud cover and hence has found wide applications including damage detection. The Haiti earthquake ($M_w=7$) on January 12, 2010 caused widespread casualty and damage to infrastructures in many parts of the country including the capital city Port-au-Prince. 217,000 people were killed making this one of the deadliest earthquakes in the modern times. Building damage detection was performed using very high-resolution pre- and post-event SAR imageries from TerraSAR-X. Radar characteristics like the correlation coefficient and the backscattering difference between the two SAR images taken in different times were calculated. To find out the building damage in the densely populated settlements as in Port-au-Prince, the threshold values of the correlation coefficient and backscattering difference were suggested and then efficiency of these thresholds was evaluated by overlaying on the optical satellite images. Building damages could be observed even in the dense urban setting of Port-au-Prince.

Keywords: The 2010 Haiti earthquake, SAR imagery, damage detection, TerraSAR-X, correlation

1. INTRODUCTION

ISDR (2010) has defined disasters as a serious disruption of a community or a society causing widespread human, material, economic and environmental losses, which exceed the ability of the community or society to cope using its own level of the resources. Radar remote sensing, as in SAR, being an active system utilizing its own energy for operation, can capture images penetrating cloud. Because of all time operation (both day and night), SAR is a very reliable source of data acquisition particularly in the times of emergency. High-resolution satellite imagery as from TerraSAR-X has opened a new facet in delivering the needs of emergency and post-disaster situation monitoring. Because of the above mentioned reasons, SAR has become a good data source to be utilized in the disaster situations including earthquakes, wildfire and so on (Matsuoka and Yamazaki 2004, 2010; Stramondo et al. 2006; Thao et al. 2010). In this paper, we analyze the damaged buildings of the Port-au-Prince city center in Haiti using high-resolution TerraSAR-X images.

2. THE HAITI EARTHQUAKE

The Republic of Haiti is located in the Caribbean Sea, occupying the western portion of the island of Hispaniola. It has little experience of earthquakes in the past. Noteworthy past earthquakes include those of 1701, 1751, 1770 and 1860 (Eberhand et al. 2010). After a large seismic gap of about 150 years, a severe earthquake of moment magnitude 7.0 hit Haiti on January 12, 2010. The epicenter of the earthquake was at Leogane, which is about 17 km from the capital city, Port-au-Prince. The depth of the earthquake was 13 km. Many cities including Leogane, Jacmel, Petit-Goave and Port-au-Prince were severely affected. Due to low preparedness and poor construction of structures, it became the most fatal event in the Haitian history: 217,000 people died, over 300,000 got injured and more than one million people were displaced. Numerous structures of national importance like presidential palace, legislative palace, national cathedral, and headquarter of United Nations, police stations, hospitals, schools, sea-port and university were severely damaged or totally collapsed. The number of

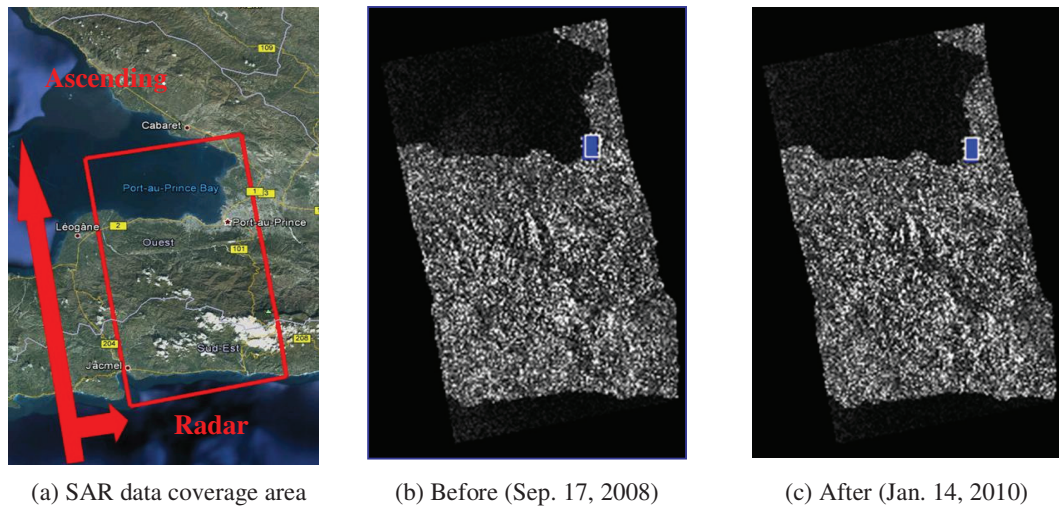


Figure 1. Location of SAR data used in this study. Red rectangle in (a) shows the geographic area covered by TerraSAR-X on Google Earth. Blue rectangles in (b) and (c) show the study area.

damaged buildings was counted as 403,176 (UNDP 2010) and the economic loss was USD 7.9 billion, which is just over 120 % of the country's gross domestic product (GDP) in 2009 (Government of Haiti 2010). The burden of the earthquake for Haiti is such that even after the 2 years of the event, a half million people are still living in tents (Reliefweb 2012) and only 5 % of the rubble (out of 19 million m³) could be removed from the streets (Time 2010).

2.1. The 2010 Haiti earthquake and SAR data

SAR data used in this research are from the TerraSAR-X satellite system (X- band, wavelength: $\lambda=31$ mm, microwave frequency: $f = 9.6$ GHz). The pre-event TerraSAR-X image used in this study was acquired on September 17, 2008 (about 15 months before the event) and the post-event image was on January 14, 2010 (2 days after the event) as shown in Figure 1. The acquisition mode of the SAR data was stripmap with HH (single) polarization. The incidence angle at the center of the images was 39.32 degrees for both. The path of the satellite was ascending with right-side look. The SAR images have ground resolution of about 3 m with the pixel size of 1.25 m. The employed data was the standard product (2A), which was radiometrically corrected, sensor corrected, geometrically corrected and mapped to a cartographic projection by the data provider: DLR.

Besides the SAR data, optical high-resolution satellite images were also used for validation. A pre-event image was from QuickBird (QB) acquired on Feb. 4, 2009 while post-event images were from GeoEye on Jan. 13, 2010, WorldView-2 on Jan. 15, 2010, and images from Google Earth.

2.2 Damage detection methodology

The study area was chosen in the downtown of the capital city, covering the most visible damage like the presidential palace and an area both common in the optical and radar imageries. After selecting the study area, an accurate positioning of the two SAR images was carried out. These images were re-sampled by changing the pixel size from 1.25 m to 0.6 m so that they can be compared to high-resolution pan-sharpened optical images. Lee adaptive filter (Lee 1980) with a 21x21 pixel window was applied to the SAR images for speckle removal.

First, the TerraSAR-X intensity images were transformed to a Sigma Naught (σ_0) value, which represents the radar reflectivity per unit area in the ground range (Breit et al. 2010; Infoterra 2008). The backscattering coefficients then obtained from the pre- and post-event SAR images have been used for change/damage detection (Yonezawa and Takeuchi 2001; Matsuoka and Yamazaki 2005,

2007). We also calculated backscatter characteristics like the backscattering difference (d) and the correlation coefficient (r) within a 21×21 pixel window of the pre- and post-event images using Eqns 1 and 2. Figure 2 shows the calibrated images of the study area.

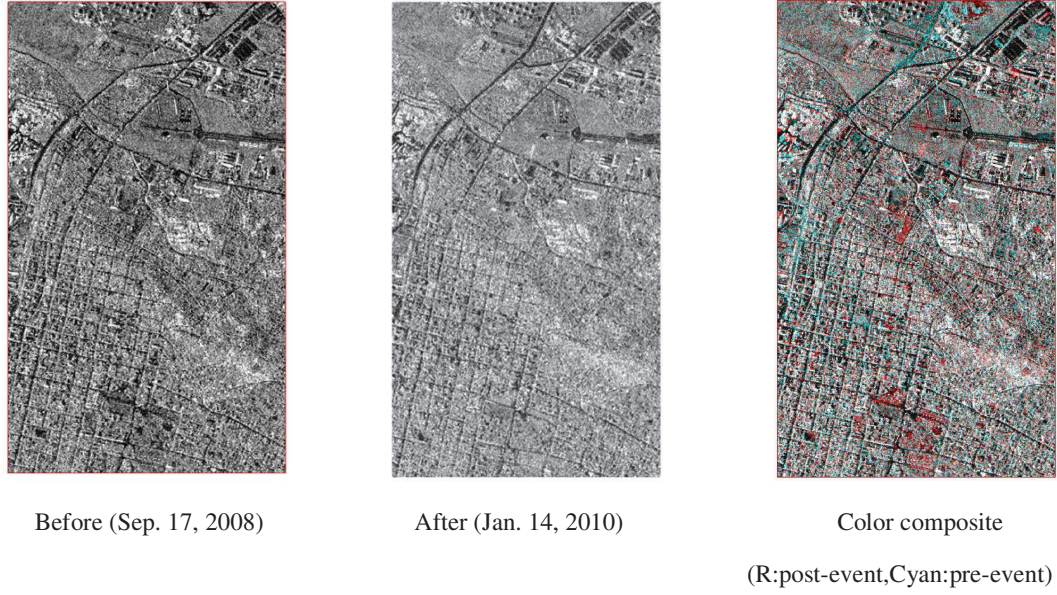


Figure 2. Radiometrically calibrated TerraSAR-X images of the study area.

$$d = \bar{I}a_i - \bar{I}b_i \quad (1)$$

$$r = \frac{N \sum_{i=1}^N I a_i I b_i - \sum_{i=1}^N I a_i \sum_{i=1}^N I b_i}{\sqrt{\left(N \sum_{i=1}^N I a_i^2 - \left(\sum_{i=1}^N I a_i \right)^2 \right) \cdot \left(N \sum_{i=1}^N I b_i^2 - \left(\sum_{i=1}^N I b_i \right)^2 \right)}} \quad (2)$$

where $I a_i$ and $I b_i$ represent the i -th pixel values of the post-event and pre-event images, respectively and $\bar{I} a_i$ and $\bar{I} b_i$ are the average values for 21×21 pixels surrounding the i -th pixel.

Finally, the threshold values of the correlation coefficient (r) and the backscattering difference (d) were selected by a trial and error method to estimate the building damage distribution. The threshold values used are $r \leq 0.25$ as low correlation and $d \leq -4$ dB and $d \geq 4$ dB as high backscatter differences. The Normalized Density Vegetation Index (NDVI) was calculated from the pre-event QuickBird image to characterize vegetated and artificial land cover areas. A low NDVI value (≤ 0.1) was utilized for excluding vegetation in the study area.

The accuracy of damage detection from the pre- and post-event SAR images was evaluated by overlying the extracted results on different urban settings, which are low-, moderate- and high- density areas determined from the optical satellite images. For the low- and moderate-density areas, damages to each building (Grades 3, 4 and 5) were transferred from the post-disaster need assessment (PDNA) survey atlas to a GIS environment. The PDNA atlas was prepared by UNITAR/UNOSAT in collaboration with different agencies including the World Bank (UNITAR et al. 2010). Building polygons in the sample areas were drawn over the satellite images. The threshold values from NDVI, r and d were overlaid on the building footprints and an area ratio was calculated to determine the percentage covered by the combined thresholds of the backscatter characteristics and NDVI.

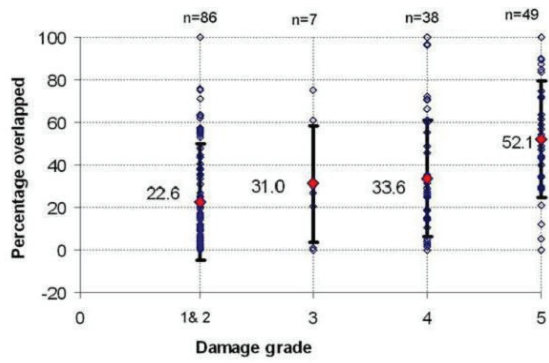


Figure 3. Graph showing the percentage of overlaid areas of the NDVI and backscatter characteristics thresholds to the building footprints of different damage grades. Error bar is drawn for each mean value with 1 standard deviation. n is the number of buildings in each grade.

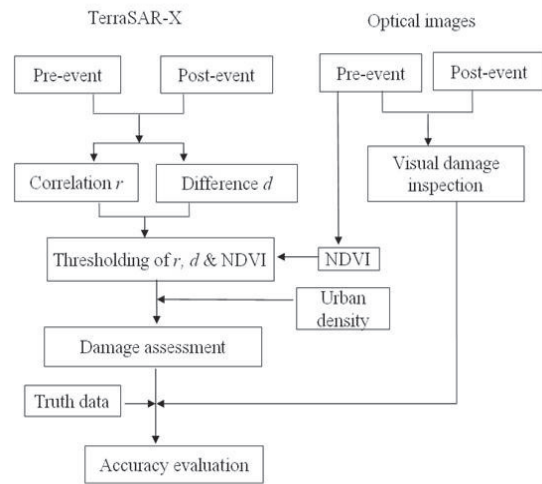


Figure 4. Flow chart of methodology adopted in this study.

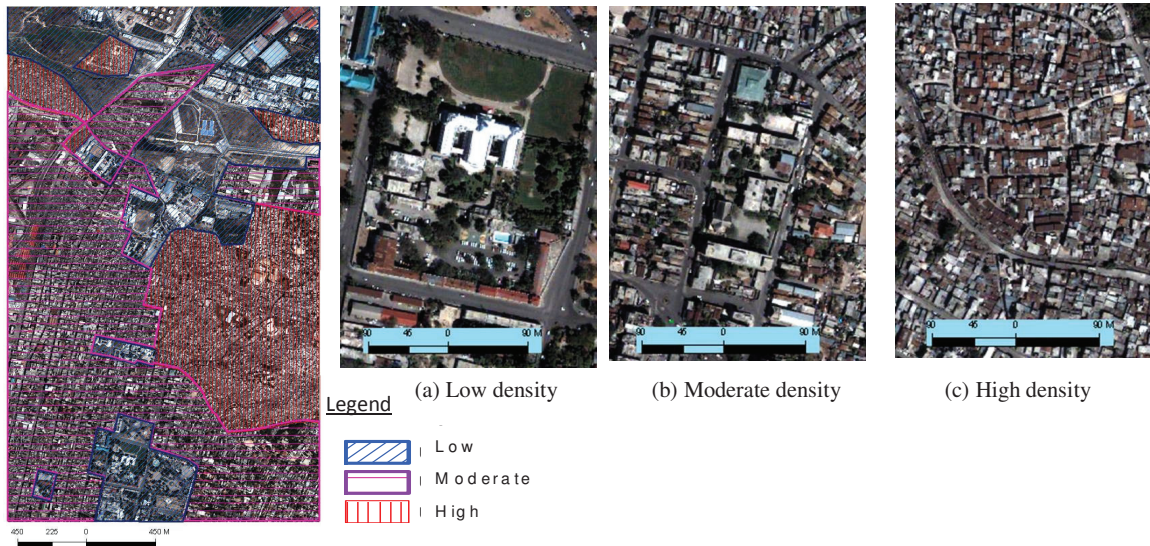


Figure 5. Classification of the study area based on urban density. Example of each class is given (a) low-, (b) moderate-, and (c) high-density areas.

Figure 3 shows the result of percentage of the overlaid areas of the threshold backscatter characteristics upon the building footprints of different damage grades based on the EMS scale. The Grades 3, 4 and 5 are damaged buildings while Grades 1 and 2 represent less-damaged buildings. Based on Figure 3, the threshold value of 43% was taken for the damage detection. If the combined area of the overlapped backscatter characteristics is equal or less than 43% of a building footprint then the building will be judged as less-damaged otherwise damaged. For this purpose, we divided buildings into 2 groups, namely damaged buildings (Grade 5) and less-damaged buildings (Grades 1-4).

Regarding the high-density area, an area-based damage estimation was carried out. For this purpose, we calculated the backscattering characteristics for the sampled block and a combined area of the overlapped threshold values from NDVI, r and d was extracted. The percentage of the probable damage areas was then calculated Figure 4 shows the flowchart of methodology adopted in this study.

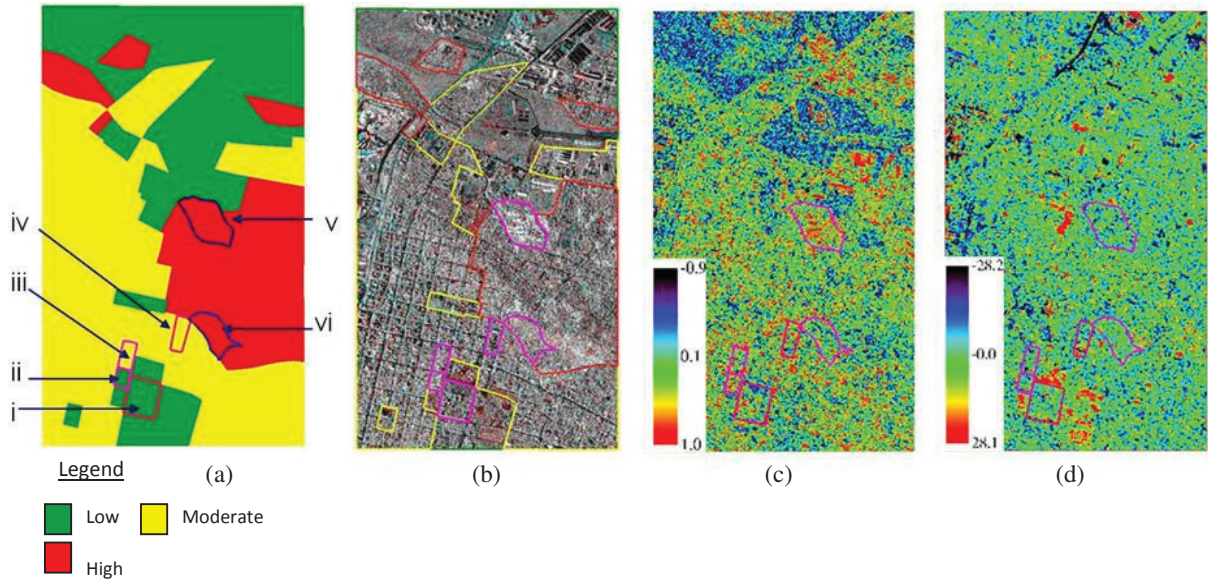


Figure 6. (a) Urban density of study area. Sampled areas in each density class are marked from (i) to (vi), (b) Color composite (Red: post-event, Cyan: pre-event), (c) Correlation map, and (d) Backscattering map.

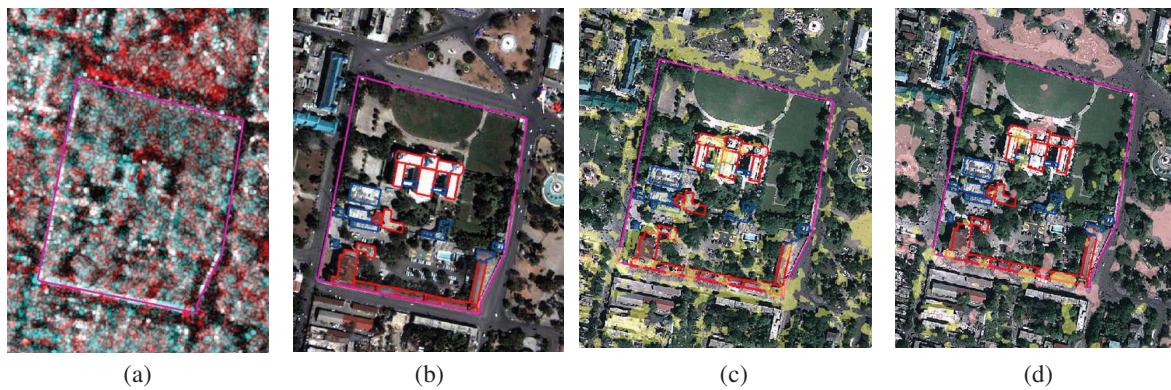


Figure 7. Example of low-density area (Area i in Figure 6(a)). (a) Color composite (Red: post-event, Cyan: pre-event), (b) Pre-event QuickBird image, (c) Post-event GeoEye image with damaged buildings in red color polygons and subsequent overlay of low correlation, $r \leq 0.25$ and $NDVI \leq 0.1$, and (d) Overlay of high backscatter difference, $d \leq -4$ dB & $d \geq 4$ dB: yellow color shows high negative d while orange color is high positive d .

Figure 5 shows the classification of the study area based on urban density. Example of each class is given in the inset. Figure 6 shows the result of urban classification and the corresponding color composite, correlation and backscattering maps. Figure 6(a) shows the urban density and the sampled areas of each density class while Figure 6(b) is the color composite of the calibrated SAR images (red: the post-event, cyan: the pre-event). Red color marks increased backscatter due to possible changes in the aftermath of the earthquake; cyan areas represent decreased backscatter while grey areas are the unchanged areas over the time. Likewise, Figure 6(c) and Figure 6(d) are the correlation and backscattering difference plots, respectively. The correlation coefficient value ranges from -0.9 to 1 while the backscattering coefficient difference ranges from -28.1 to 28.2 dB in this sampled area.

When we overlay the union of threshold $NDVI \leq 0.1$ and backscatter characteristics ($r \leq 0.25$ and $d \leq -4$ dB & $d \geq 4$ dB) in a low density area including the presidential palace (Figure 7), it was found that out of 10 damaged building footprints (Grade 5), 7 building footprints had the threshold areas of more

than 43%. As discussed in the methodology section, they represent the damaged buildings. Similarly, 13 out of 16 less-damaged buildings could be correctly identified. It is to be noted that less-damaged buildings were also identified as damaged buildings. Radar backscatter is affected by the satellite path, building layout and even vegetation. When the orientation of a tall building is facing to the radar path, then the adjacent short buildings are affected by it. This may happen to the main building in the presidential complex and a less-damaged building was identified as damaged.

Similarly, if we overlay the union of threshold values of NDVI (≤ 0.1), low correlation ($r \leq 0.25$) and high backscatter difference ($d \leq -4$ dB & $d \geq 4$ dB) in moderate-density areas as in Figure 8, we noticed that out of 2 damaged buildings, none of them could be correctly identified by our damage criteria (the overlay percentage of the union of the threshold values within a building footprint $\leq 43\%$ as less-damaged and more than it as damaged). However, out of 27 less-damaged buildings, 27 could be correctly recognized. Table 1 shows the error matrix of the low- and moderate-density areas. Out of 33 damaged buildings, 22 buildings could be correctly identified while out of 131 less-damaged buildings 99 buildings were correctly identified. The producer's accuracy for the damaged buildings is 66.7% while the user's accuracy is 40.7%. The overall accuracy is 73.8%.

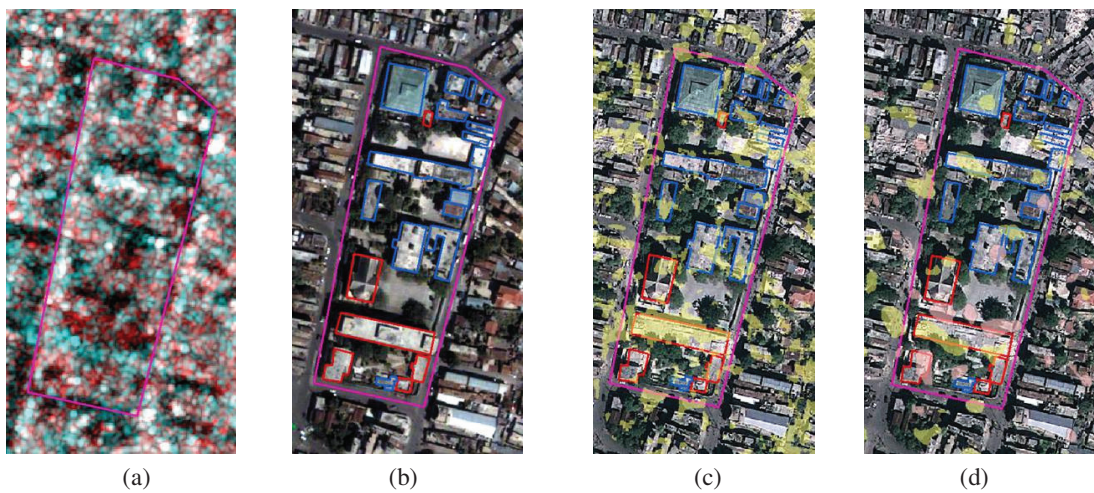


Figure 8. Example of moderate- density area (Area iv in Figure 6(a)). (a) Color composite (Red: post-event, Cyan: pre-event), (b) Pre-event QuickBird image, (c) Post-event GeoEye image with damaged buildings in red color polygons and subsequent overlay of low correlation, $r \leq 0.25$ and $NDVI \leq 0.1$, and (d) Overlay of high backscatter difference, $d \leq -4$ dB & $d \geq 4$ dB: yellow color shows high negative d while orange color is high positive d .

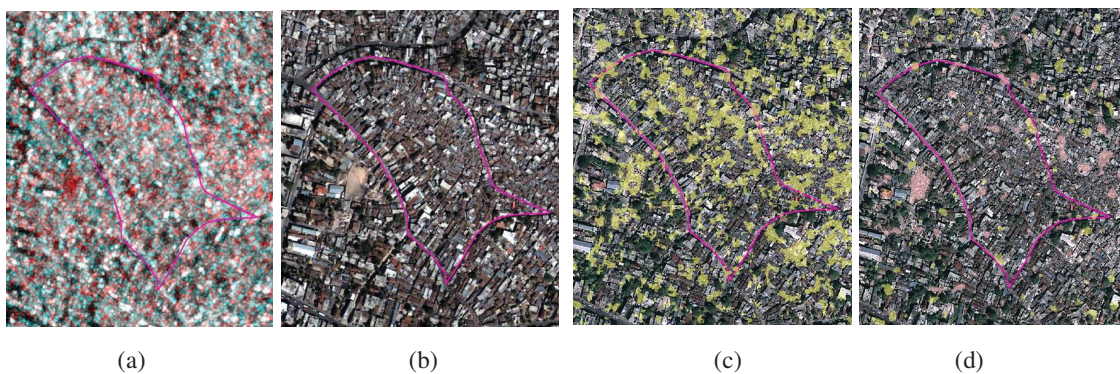


Figure 9. Example of high-density area (Area vi in Figure 6(a)). (a) Color composite (Red: post-event, Cyan: pre-event), (b) Pre-event QuickBird image, (c) Post-event GeoEye image and subsequent overlay of low correlation, $r \leq 0.15$ and $NDVI \leq 0.1$, and (d) Overlay of high backscatter difference, $d \leq -4$ dB & $d \geq 4$ dB: yellow color shows high negative d while orange color is high positive d .

Table 1. Error matrix for low- and moderate-density areas

	Damaged (G5)	Less-damaged (G1-G4)	Sum	User's accuracy (%)
Damaged (G5)	22	32	54	40.7
Less-damaged (G1-G4)	11	99	110	90.0
Sum_PDNA	33	131	164	
Producer's accuracy (%)	66.7	75.5		
Overall accuracy (%)				73.8

Regarding high-density areas as in Figure 9, the total area covered by low correlation ($r \leq 0.15$) and high backscatter difference ($d \leq -4\text{dB}$ & $d \geq 4\text{dB}$) in the two sampled blocks is 31, 693.79 m² while the blocks have area of 150, 290.05 m². So the possible damage area is about 21%. The reason of the low detection ratio from the SAR imagery might be explained by the high density of this study area. It is to be mentioned that although we used the PDNA's result as the truth data, it was produced from visual inspection of satellite and vertical aerial images. Therefore, survey data from the ground is necessary for more detailed evaluation.

3. CONCLUSION

We used pre- and post-event high-resolution TerraSAR-X images for detecting building damages for the 2010 Haiti Earthquake. Backscatter characteristics like the correlation coefficient and the backscattering difference were calculated from the pre- and post-event intensity images. Building damage detection was evaluated for three different density areas using the threshold values of the correlation coefficient and the backscatter difference. Damaged buildings were effectively detected with overall accuracy of 73.8% for the low- and moderate-density areas based on low correlation coefficients and high backscatter differences. However, it was not so high accuracy for high-density areas because building damages were not so much visible from the top view of the areas. Even though some limitations still remain, the results from this study show the usefulness of high-resolution SAR intensity images in building damage detection even in densely buildup areas such as Port-au-Prince.

ACKNOWLEDGEMENT

The TerraSAR-X images used in this study were made available from SAR Application Research Committee, organized by PASCO Corporation, Tokyo, Japan.

REFERENCES

- Breit, H., Fritz, T., Balss, U., Lachaise, M., Niedermeier, A., and Vonavka, M. (2010). TerraSAR-X SAR processing and product. *IEEE Transaction on Geoscience and Remote Sensing*.**48:2**, 727-740
- Eberhard, M.O., Baldrige, Steven., Marshall, Justin., Mooney, Walter., and Rix, G. J. (2010). The MW 7.0 Haiti earthquake of January 12, 2010. USGS/EERI advance reconnaissance team report: U.S. geological survey open-file report 2010-1048, 58.
- Infoterra. (2008). Radiometric Calibration of TerraSAR-X data.
- ISDR. (2010). <http://www.unisdr.org/eng/library/lib-terminology-eng%20home.htm>.
- Lee, J. S. (1980). Digital image enhancement and noise filtering by use of local statistics. *IEEE Transaction, Pattern Analysis and Machine Intelligence, Photographic Surveying and Remote Sensing* **2:2**, 165-168.
- Government of Haiti. (2010). Action plan for national recovery and development of Haiti.
- Matsuoka, M., and Yamazaki, F. (2004). Use of satellite SAR intensity imagery for detecting building areas damaged due to Earthquakes. *Earthquake Spectra* **20:3**, 975-994.
- Matsuoka, M., and Yamazaki, F. (2005). Building damage mapping for the 2004 Nigata-ken Chetsu earthquake using Radarsat images. *Earthquake Spectra* **21:SI**, 285-294.

- Matsuoka, M., Yamazaki, F., and Ohkura, H. (2007). Damage mapping for the 2004 Nigata-ken Chetsu earthquake using Radarsat images, *Urban Remote Sensing Joint Event IEEE*, Paris, France, CD-ROM.
- Matsuoka, M., and Yamazaki, F. (2010). Comparative analysis for detecting areas with building damage from several destructive earthquakes using satellite synthetic aperture radar images. *Journal of Applied Remote Sensing SPIE*, **4:1**, 1-16.
- Reliefweb. (2012).
http://www.reliefweb.int/sites/reliefweb.int/files/resources/Full_Report_3325.pdf
- Stramondo, S., Bignami, C., Chini, M., Pierdicca, N., and Tertulliani, A. (2006). Satellite radar and optical remote sensing for earthquake damage detection: results for different case studies. *International Journal of Remote Sensing* **27:20**, 4433-4447.
- Thao, N.V., Lan, D. T., Huong D.T., and Ve, N.D. (2010). Assessing damage of flood by using ALOS data in Thua Thien-Hue Province. *The 4th Joint PI symposium of ALOS Data nodes for ALOS Science Program* Tokyo, Japan, 125.
- Time. (2012).
<http://www.time.com/time/world/article/0,8599,2041450,00.html#ixzz1jspmAwn>
- United Nations Institute for Training and Research (UNITAR), Operational Satellite Applications Programme (UNOSAT), European Commission (EC). Joint Research Centre (JRC) and The World Bank. (2010). Atlas of building damage assessment Haiti earthquake 12 January 2010 in support to post disaster needs assessment and recovery framework (PDNA).
- United Nations Development Programme. (2010).
<http://www.ht.undp.org/?lang=en&PHPSESSID=c3a4637485efbb3623ee7dca511280b3>.
- Yonezawa, C. and Takeuchi, S. (2001). Decorrelation of SAR data by urban damages caused by the 1995 Hyogoken-nanbu Earthquake. *International Journal of Remote Sensing* **22:3**, 1585-1600.